

# 14

# A NEW REVERSIBLE HIGH-SPEED FRINGE COUNTER FOR LASER INTERFEROMETRY (\*)

F. T. ARECCHI - G. LEPRE - A. SONA (\*\*) 257131

Long distance interferometry is now possible using a laser as source. Fringe systems with high visibility have been observed on a Michelson interferometer with an optical path difference up to 120 m using a He-Ne c.w. visible gas laser in single mode operation. The interferometer can be operated either with fixed mirrors for stability measurements or with a movable mirror for an absolute length measurement.

Both measurements require an accurate reversible fringe counter to yield information on the absolute change in the optical path difference.

The electronic system which yields such information is described in detail with particular emphasis on the following points:

- a) logic of the circuitry;
- b) band-width and speed limits due to noise for low level light detection;
- c) high-speed reversible counter with analog and digital output.

Some preliminary results of stability measurements are given. The performance can be summarized as follows:

$\lambda/8$  resolution without fringe interpolator,  $10^3$  pulses/s or better depending on the source strength.

of measurements, namely:

- a) stability measurements of a standard base;
- b) length measurements.

In both cases the experimental set-up is as shown in fig. 1. The laser output is splitted by a beam splitter  $M_1$  onto a Michelson interferometer through a telescope system which reduces the angular spread. The two Michelson mirrors  $A$  and  $B$  are made by two cat's eye systems for easier alignment. This allows to span a long distance on a conventional optical bench without re-adjusting the system. The fringe system is sent to a pair of photomultipliers P.M.1 and P.M.2 through annular diaphragms  $D_1$  and  $D_2$  concentric to the fringe system and narrower than the fringe spacing. The two diaphragms select two regions of the fringe pattern dephased in space by about  $90^\circ$  in order to obtain information both on the number of fringes which are crossing the apertures and on the sense of the movement. An improved system, proposed by Peck and Obetz [2], to obtain two  $90$  degree dephased signals is now being tested. If the position of the two mirrors is fixed, the difference between the number of counts in one sense and the other yields

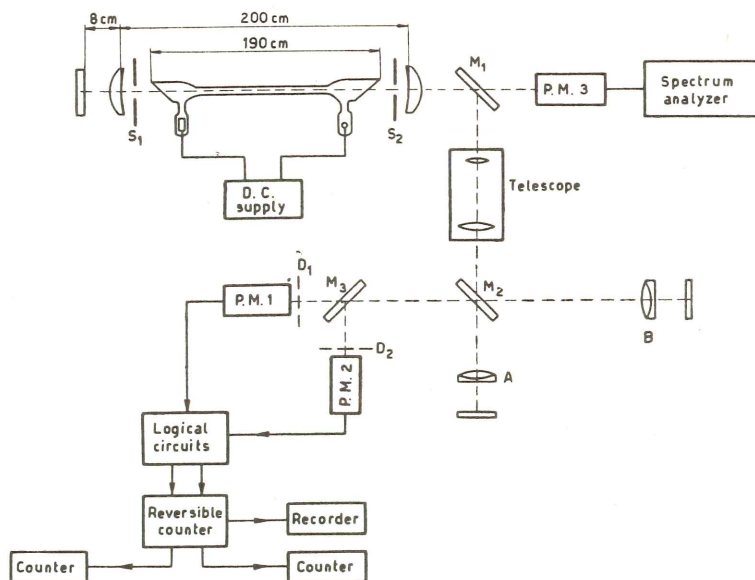


Fig. 1. — Experimental set-up.

## I. — INTRODUCTION.

Long distance interferometry using a gas laser as source has been reported [1] as promising for two sets

(\*) Work done with the financial support of the C.N.R.

(\*\*) F. T. ARECCHI, G. LEPRE, A. SONA, CISE Labs. Milano - Italy.

a stability information. If one of the mirrors is moved, the associated counter yields a digital measurement of the spanned length.

As said in the analysis of ref. [3] the elastic vibrations in the acoustic range of the interferometer frame and the atmospheric scattering (turbulence and brownian motion) reduce the resolving power. If we consider the

whole measuring instrument (interferometer plus electronics), the circuit noise also contributes to reducing the whole resolving power.

We shall give a set of considerations for handling the signals of the phototubes in order to obtain stability and length measurements, and to minimize noise effects.

In the working range defined below, we obtain a length resolution of  $\lambda/8$  against  $\lambda/2$  of previous works [4] [5], without using analog interpolators, and a counting speed of  $10^5$  p/s against the 1200 p/s of ref. [5].

2. - LOGIC OF THE OPERATION.

The operation of the interferometer can be analyzed looking at the Lissajous pattern which appears at an oscilloscope whose *X* and *Y* inputs are connected to the phototubes (fig. 2a). A whole turn corresponds to a

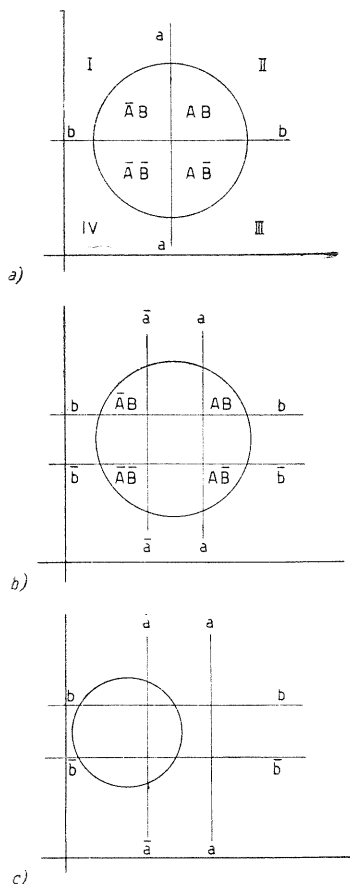


Fig. 2. -- Lissajous patterns built with the two phototube outputs: *a-a* and *b-b* threshold lines of the discriminators.

path shift of  $\lambda$  and therefore to an effective relative shift of the mirrors of  $\lambda/2$ . The instantaneous position of the spot on the Lissajous circle is a function of the path difference, with period  $\lambda$ . The sense of movement of the spot corresponds to the sense of motion of the moving mirror. Two trigger circuits are associated to the two phototubes and change their state every time the spot crosses the threshold level (respectively, *a-a* for channel *A*, and *b-b* for channel *B*). Let us call *A* and  $\bar{A}$  the ON and OFF states of the discriminator *A*; *A'* and  $\bar{A}'$  the transitions  $\bar{A} \rightarrow A$  and  $A \rightarrow \bar{A}$ ; and do the same with *B*. When the two threshold lines cross within the Lissajous circle, we have a set of 8 parameters, 4 associated with stationary states and 4 with transitions.

When the interferometer is in a stable position, the corresponding representative point will be in one of the 4 quadrants, and will be localized by two stationary parameters. When one mirror is moving with respect to the other, the motion is defined by the 4 crossing of the *a-a* and *b-b* diameters. These crossings are represented by the combination of the stationary state of one discriminator with the transition of the other. A full clockwise rotation of the spot, starting from the first quadrant, will give rise to the following series of events:

$$B A', A \bar{B}', \bar{B} \bar{A}', \bar{A} B'$$

where each pair of letters denotes an AND operation associated to the switching of quadrant, the first letter corresponding to the state of the discriminator which does not change and the second to the transition of the other discriminator. Similarly, a full counter-clockwise rotation will give rise to the following events:

$$\bar{A} \bar{B}', \bar{B} A', A B', B \bar{A}'$$

The first set of signals is logically summed onto an output *X* and the second onto an output *Y*. So a train of pulses is obtained from *X* and *Y*, for clockwise and counterclockwise rotations respectively.

One can easily see that, for any fluctuation on the interferometer around a stable position, the oscillating Lissajous spot yields an equal number of counts at the two outputs *X* and *Y*. Therefore the counts difference is unaffected by spurious fluctuations with zero average, and changes by 1 every time there is an effective path difference of  $\lambda/4$ , corresponding to a  $\lambda/8$  shift in the moving mirror.

The hysteresis inherent to the discriminators splits the switching levels introducing an imprecision smaller than the resolving power  $\lambda/8$  (fig. 2b). Therefore the system is insensitive to hysteresis effects, unless a situation topologically equivalent to fig. 2c occurs. Here one of the two discriminators can no more switch and the *X-Y* output has zero average, independently on the sense of the movement of the point on the Lissajous pattern.

These considerations are still valid when the two signals on the phototube are no more equal in amplitude or out of  $90^\circ$ , that is when the Lissajous is no more a circle, unless the topological equivalent of fig. 2c occurs.

3. - ANALYSIS OF THE CIRCUITRY.

The block diagram of the circuitry is shown in fig. 3. One of the trigger sections (fig. 4) is made of three emitter followers  $T_1, T_2$  and  $T_3$  followed by a regenerative loop  $T_4, T_5$  which acts as current-driven amplitude discriminator. A direct cascade of complementars common base and common collector stages is known as hook transistor connection [4]. When the input current  $i_s$  is below threshold,  $T_1$  and  $T_5$  are off. As soon as  $i_s$  drives  $T_4$  into conduction, a positive feedback pushes  $T_4$  and  $T_5$  toward saturation. The discriminator switches back to the initial condition when the input falls down to a level fixed by the diode  $D_1$  and the potentiometer  $P_2$ . The threshold and hysteresis can be regulated respectively through the potentiometers  $P_1$  and  $P_2$ . This is particularly important, as the noise analysis will show below.

The trigger section is followed by delay line differentiators and amplifying and inverting stages, to yield the 8 signals  $A, \bar{A}, B, \bar{B}$  and  $A', \bar{A}', B', \bar{B}'$  as normalized

The  $X$  and  $Y$  pulses are sent to a reversible decimal counter which yields the counts difference as digital output (neon lamps) and analog output sent to a chart

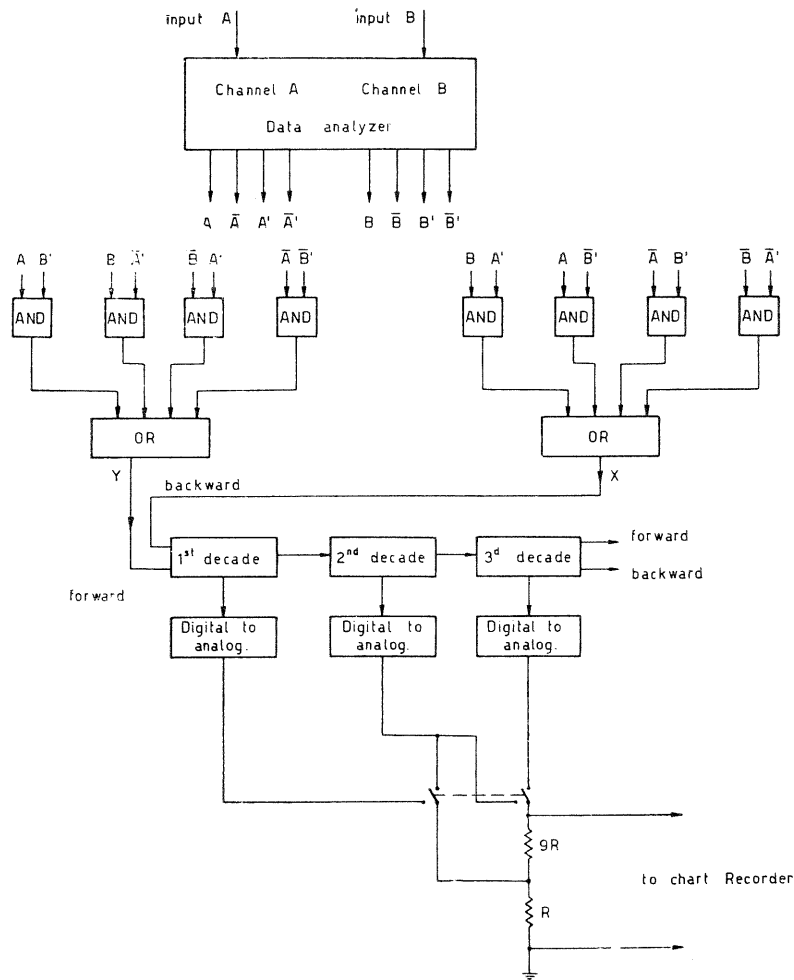


Fig. 3. — Block diagram of the circuitry.

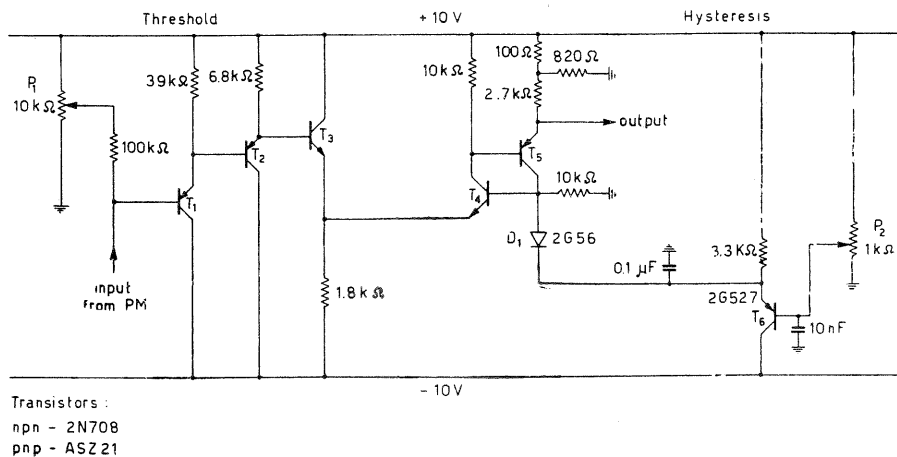


Fig. 4. — Amplitude current-driven discriminator.

outputs. These outputs, through AND and OR circuits, build up the two signals:

$$X = B A' + A \bar{B}' + \bar{B} \bar{A}' + \bar{A} B'$$

$$Y = \bar{A} \bar{B}' + \bar{B} A' + A B' + B \bar{A}'$$

recorder (through a suitable converter). In fig. 5 we report the scheme of the reversible counter which seems different and simpler than previous types [6]. The maximum speed in one sense is  $10^6$  counts/s, in both senses better than  $10^5$  counts/s, and is limited by the charging

time of the commuting capacitors. The reversible counter is made by three decades which transfer their overflow to a pair of conventional counters, to record respectively

40  $\mu$ , and its output is recorded for convenience in analog form on a strip chart recorder. In the measurement of a spanned length, one reads the thousands of

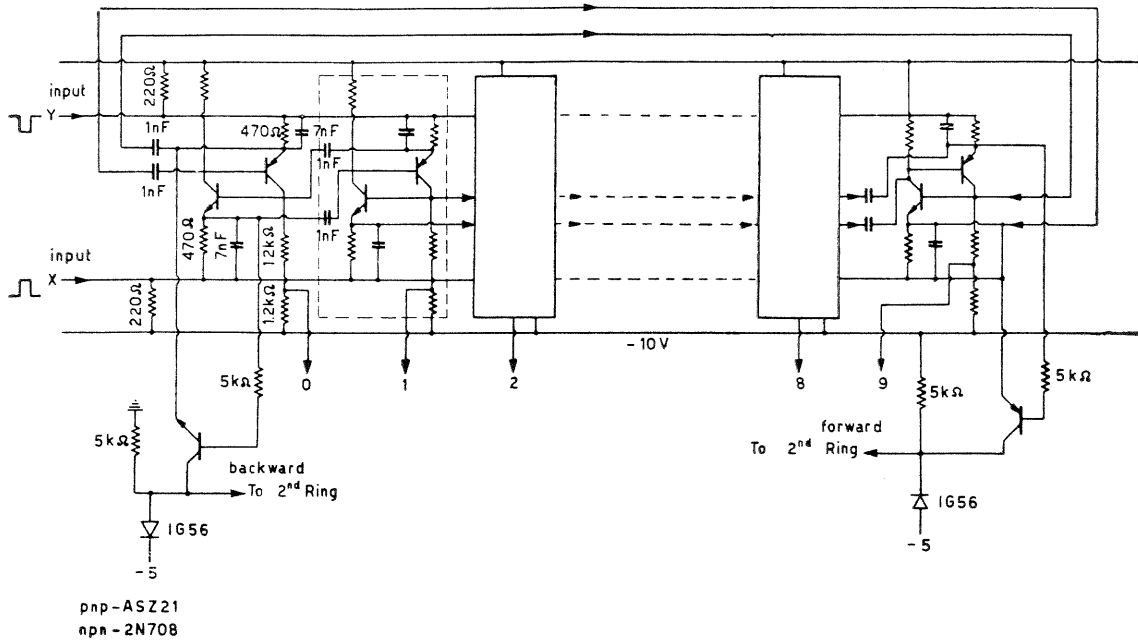


Fig. 5. — Reversible counter.

the thousands of counts in one sense or the other. Each decade is made by 10 hook transistor connections (fig. 5) driven at the two inputs by a further pulse-forming hook transistor pair (fig. 6). The pulse former has the

$\lambda/8$  on the auxiliary decimal counter which has been operated, and the hundreds, tens and units of  $\lambda/8$  as difference in the indication of the reversible counter before and after the experiment.

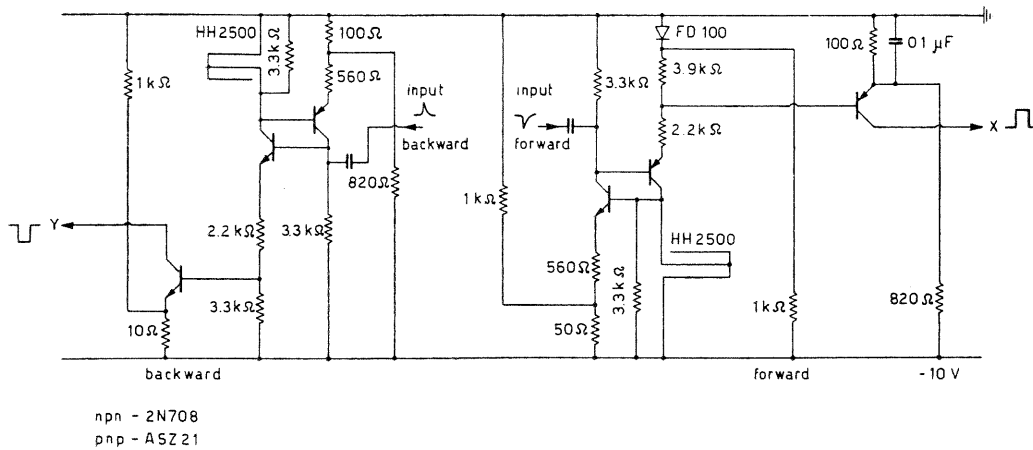


Fig. 6. — Pulse former.

advantage of a short recovery time (0.5  $\mu$ s) and of a definite pulse shaping at 0.3  $\mu$ s.

It should be noticed the extensive use that we have made of a hook circuit. This circuit had been studied already [7]; some applications were proposed in a recent work [8], and its use in a circuit scheme like in fig. 4 (amplitude discriminator with independent setting of threshold and hysteresis) or in fig. 6 (pulse former) and fig. 5 (high speed bidirectional ring counter) is done here for the first time. In a stability measurement only the reversible counter is effective up to a maximum fluctuation in one sense or the other of 500  $\lambda/8$ , that is about

#### 4. — NOISE CONSIDERATIONS AND LIMITS FOR THE COUNTING SPEED.

The noise contributes a thickness to the Lissajous circle (fig. 7a) and two considerations put limits on it:

a) the thickness of the circle should never be such as to make possible a random pattern within it, which acts as in fig. 2c.

b) The thickness and correspondingly the r.m.s. noise should not arise above the hysteresis level, in order to minimize the noise triggered switches.

Otherwise the phototube noise can induce successive

switches of the discriminator in a time shorter than the dead time of the following reversible counter. This last dead time is  $\tau_2 \cong 10 \mu\text{s}$  against  $\tau_1 \cong 1 \mu\text{s}$  of the logics.

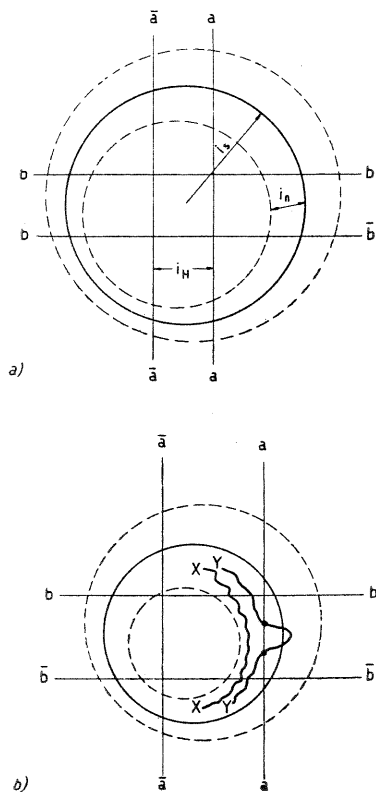


Fig. 7. — Noise contributions to the Lissajous pattern.

The two limitations can be summarized as follows:

$$(1) \quad i_s - \alpha i_n > i_H/2 > \beta i_n$$

where:

$i_H$  is the hysteresis current,

$i_n$  is the r.m.s. output noise from the photomultiplier tube,

$i_s$  is the signal current,

$\alpha$  and  $\beta$  are shape factors defined in the following.

The noise current at the anode of a photomultiplier is given by:

$$(2) \quad i_n = \sqrt{2 e G I_0 f_1 \delta / (\delta - 1)}$$

where:

$f_1$  is the bandwidth of the electronics before the discriminators, which in our case coincides with the bandwidth of the logic,

$\delta$  is the secondary multiplication factor of the dynodes,  
 $G$  is the phototube gain,

$I_0$  is the d.c. component of the phototube current at the threshold level of the discriminator.

The signal current  $i_s$  is related to the d.c. component  $I_0$  through the fringe visibility  $V$ . Namely (fig. 8):

$$(3) \quad V = \frac{I_{Max} - I_{Min}}{I_{Max} + I_{Min}} = \frac{i_s}{I_0}$$

Relation (1) becomes:

$$(1') \quad i_s - \alpha \sqrt{2 e G \frac{\delta}{\delta - 1}} \sqrt{\frac{i_s}{V} f_1} > \frac{i_H}{2} > \beta \sqrt{2 e G \frac{\delta}{\delta - 1}} \sqrt{\frac{i_s}{V} f_1}$$

These boundaries limit the region of possible values for  $i_H$ . Some considerations must be done about  $\beta$  and  $\alpha$ .

a) calculation of  $\beta$ .

As already stressed, the electronics is made by cascading two different sets of circuits: the logic, with a band-

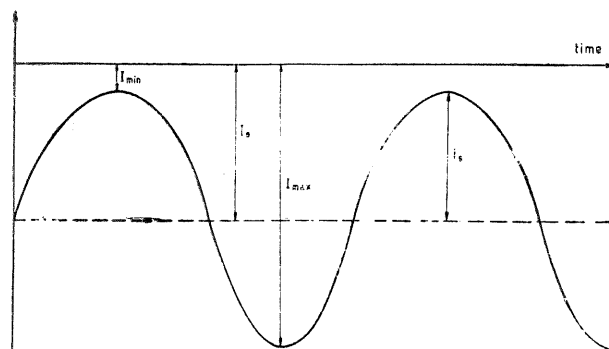


Fig. 8. — Relations between visibility  $V$ , signal current  $i_s$ , and d.c. component  $I_0$ .

width  $f_1$  and a corresponding dead time for counting  $\tau_1 = 1/2 f_1$  and the reversible counter with a dead time  $\tau_2 = 1/2 f_2$ . The average rate of noise pulses can be measured on one channel for different values of  $i_H$  around  $I_0$  and comes out to be given by:

$$(4) \quad f = 2 f_1 e^{-\left(\frac{1}{2\sqrt{2}} \frac{i_H}{i_n}\right)^2}$$

as results from the experimental plot of the fig. 9.

The probability of more than one pulse on the same channel within the time  $\tau_2$  is given by:

$$(5) \quad p \cong f \tau_2$$

because we shall design the  $i_H$  values such as that  $f \tau_2 \ll 1$ . The number of wrong counts per second due to noise is given by (4) and (5) (1):

$$(6) \quad n = f p = f^2 \tau_2$$

Furthermore any fluctuation in the optical path with zero average will give an extra number of counts per second  $F$ . These fluctuations can be originated both by atmospheric turbulence and length fluctuations. They cannot be distinguished from each other unless additional

(1) Furthermore, the average repetition rate should be reduced by a filling factor

$$\eta \cong \frac{4 i_H}{2 \pi i_s}$$

corresponding to the probability for the Lissajous spot of being in the hysteresis region. But for the sake of simplicity we shall assume  $\eta = 1$ , which is the least favorable condition.

hypothesis are made on their respective spectral distributions.

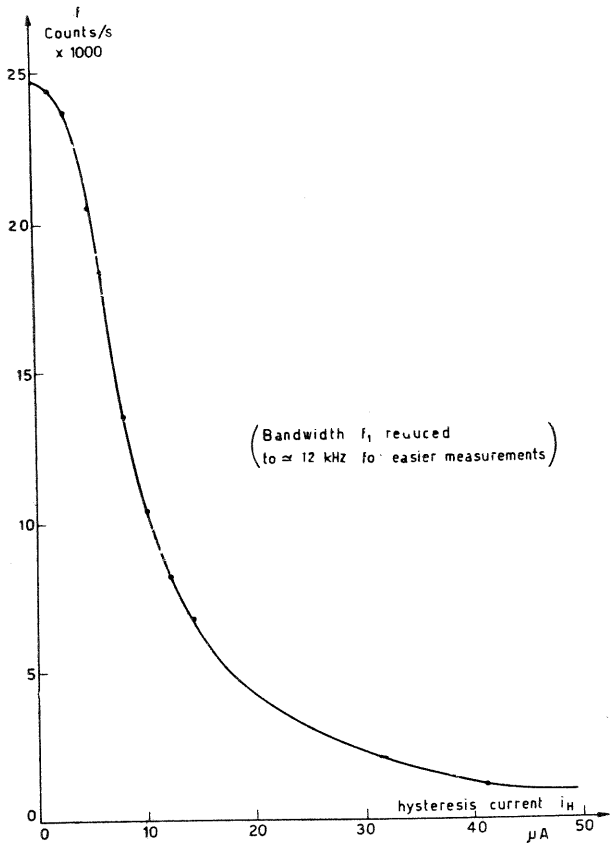


Fig. 9. — Experimental plot of the frequency of noise counts vs. hysteresis current.

The total number of wrong counts per second in the counter is then given by:

$$(7) \quad n = (f + F)^2 \tau_2$$

As the wrong counts occur with the same probability in both senses, they give rise to a random walk in the position of the counter. After a time  $T$  sec the position of the counter will be shifted from the correct one of a quantity which has zero average over a number of equally repeated measurements and a variance  $\sqrt{n T}$ . A consequent error arises in the measurement, because after a time  $T$  the position of the counter is affected by a standard deviation  $(f + F) \sqrt{\tau_2 T}$ .

The ultimate precision of this measurement is given by  $F \sqrt{\tau_2 T}$ . The extra error  $f \sqrt{\tau_2 T}$  caused by the electronics can be minimized by setting the hysteresis at a level such that  $f < F$ . From (4), this condition corresponds to

$$(8) \quad \frac{i_H}{i_n} > 2 \sqrt{2} \sqrt{\ln 2 \frac{f_1}{F}} = 2 \beta$$

For instance, let us consider two different external conditions, with  $F = 10^2 \text{ s}^{-1}$  and  $F = 10^3 \text{ s}^{-1}$  respectively. Since in our system  $f_1 = 10^6 \text{ s}^{-1}$ , we obtain for  $\beta$  respectively  $\beta = 3.9$ , and  $\beta = 4.5$ . Condition (8) can be fulfilled either by increasing  $i_H$  or by decreasing  $i_n$  (limiting the bandwidth  $f_1$  with an input filter).

b) calculation of  $\alpha$ .

As regards the upper limitation, when the thickness of the Lyssajous circle allows a situation like in fig. 2c, two paths can occur, namely as the  $x-x$  line which does not intersect the switching level  $a-a$ , or as the  $y-y$  line which intersects this level at least twice (see fig. 7b).

A path like  $x-x$  gives a loss of one count, a path like  $y-y$  does not give any disturb. Now, the path  $x-x$  implies that the noise remain correlated while the spot goes from  $b-b$  to  $\bar{b}-\bar{b}$ , and therefore depends on the velocity of the moving spot.

The correlation time of the noise is of the order of  $1/f_1$ , the time for the spot to pass through the hysteresis region is of the order of the average period of the fringe variations, that is:

$$\frac{1}{F} \quad \text{in a stability measurement}$$

$$\frac{1}{F + L} \quad \text{in a length measurement}$$

where  $F$  is the frequency of fluctuations in the optical path,  $L$  is the frequency of the moving fringes when moving a mirror for a length measurement.

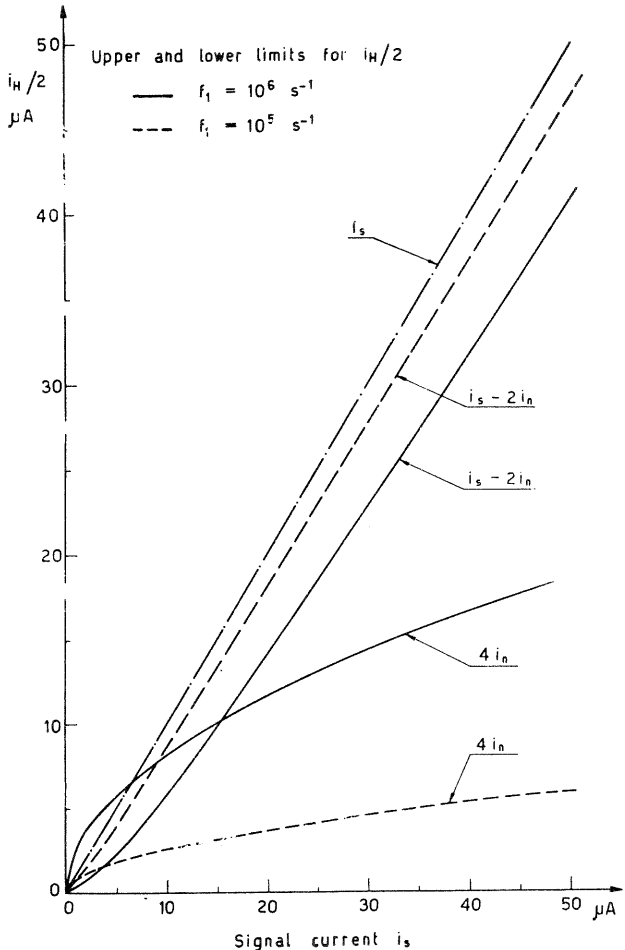


Fig. 10. — Upper and lower limitations to the hysteresis current in a stability measurement.

In the first case, since  $F = 10^{-3} f_1$ , the noise can be considered as completely uncorrelated in a time of travel

across the hysteresis band, and therefore a  $x-x$  path is highly unlikely. In this case, the upper limitation reduces to  $i_s > i_H/2$  as can be deduced from fig. 2c. In the second case, the dead time of the reversible counter, when counting only in one sense, allows a maximum useful speed of  $1/f_1$ , that is  $1/(F + L)$  at the maximum speed is of the same order as the correlation time for noise.

In this case, the correlation is almost 1, and therefore the probability of losing counts is given approximately by the probability of crossing a given level, that is

$$(10) \quad P = \epsilon \exp - \left( \frac{i_s - (i_H/2)}{\sqrt{2} i_n} \right)^2$$

This probability gives the relative precision of a measurement. In order to have it better than  $10^{-8}$  one has to use:

$$i_s - (i_H/2) > 4.3 \sqrt{2} i_n$$

that is  $\alpha \cong 6$ .

When the velocity of the moving mirror is below the maximum the probability (10) becomes

$$(10') \quad P = (L f_1) \epsilon \exp - \left( \frac{i_s - (i_H/2)}{\sqrt{2} i_n} \right)^2$$

and the limitation is less stringent, that is  $\alpha$  goes continuously down to zero as we decrease the velocity.

In a stability measurement, the number of wrong counts per second, by a reasoning similar to the one made for the lower limit, is

$$(11) \quad \bar{n} = F P$$

where  $P$  is now given by:

$$P = \frac{F}{f_1} \exp - \left( \frac{i_s - (i_H/2)}{\sqrt{2} i_n} \right)^2$$

In order that this random walk give a contribution equal or less than the one of the lower limit, it must be:

$$\frac{1}{f_1} \exp - \left( \frac{i_s - (i_H/2)}{\sqrt{2} i_n} \right)^2 < \tau_2$$

where  $\tau_2 \cong 10/f_1$ .

This yields a value  $\alpha \cong 2.1$ .

In fig. 10 we have reported upper and lower limitations  $i_s - \alpha i_n$  and  $\beta i_s$  vs.  $i_s$  for a stability measurement and for the following set of parameters:

$$F = 1, \quad G = 10^6, \quad \delta = 4, \quad \alpha = 2, \quad \beta = 4$$

and two values of frequency:

$$\begin{cases} f_1 = 10^6 \text{ s}^{-1} \\ f_1 = 10^5 \text{ s}^{-1} \end{cases}$$

*Acknowledgement.* — The authors are grateful to Prof. E. Gatti for stimulating discussions during this work.

*The paper was first received 17th June 1964.*

#### BIBLIOGRAPHY

- [1] F. T. ARECCHI, A. SONA: « Nuovo Cimento », 32, 1117 (1964)
- [2] E. R. PECK, S. W. OBETZ: « Journ. Opt. Soc. Am. », 43, 505 (1953).
- [3] F. T. ARECCHI, A. SONA: « Proc. Symposium on Quasi Optics », Brooklyn 8-10 June 1964.
- [4] H. D. COOK, L. A. MAZZETTA: « Journ. of Res. N.B.S. », 65c, 129 (1961).
- [5] F. H. BRANIN JR.: « Journ. Opt. Soc. Am. », 43, 839 (1953).
- [6] J. D. SCHMIDT: « I.R.E. 1958 Canadian Conv. Record », p. 511.
- [7] L. M. VALLESE: « Journ. Brit. I.R.E. », 18, 725 (1958).
- [8] G. LEPRE: « Alta Frequenza », 33, (1964).